INDERSCIENCE PUBLISHERS
Linking academia, business and industry through research

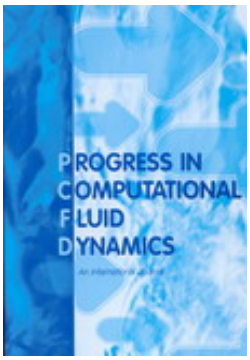

Progress in Computational Fluid Dynamics, An International Journal

ISSN online: 1741-5233 - ISSN print: 1468-4349
https://www.inderscience.com/pcfd

Numerical analysis of geometry and operating conditions in combined honeycomb and inclined labyrinth sealing elements

İbrahim Zengin, Beytullah Erdoğan

DOI: 10.1504/PCFD.2023.10053760

Article History:

Received:	10 March 2021
Last revised:	22 December 2021
Accepted:	22 December 2021
Published online:	02 February 2023

Numerical analysis of geometry and operating conditions in combined honeycomb and inclined labyrinth sealing elements

İbrahim Zengin and Beytullah Erdoğan*

Institute of Science,
Department of Mechanical Engineering,
Zonguldak Bülent Ecevit University,
Zonguldak, 67100, Turkey
Email: ibrahim.zengin@beun.edu.tr
Email: beytullah.erdogan@beun.edu.tr
*Corresponding author

Abstract: Leakage flows occurring during operating conditions within the gas turbine engine system significantly affect the turbine efficiency. It is a significant issue to control and predict the leakage flow. This study covered the labyrinth seal with inclined tooth form and honeycomb seal used together. The combined seal provides more efficient leakage flow reduction than seal designs available in the literature. The study also focused on the five different parameters affecting the leakage flow, which are clearance size (Cr = 0.254-0.508-1.016 mm), honeycomb cell size (Lcell = 0.793-1.590-3.175 mm), pressure ratio (π = 1.5-2.0-2.5-3.0), rotor speed (Vr = 0-100-200-400 m/s), and tooth inclination angle (θ = 90°-70°-50°). These parameters were investigated comprehensively with ANSYS – Fluent, which uses the finite volume method. Results showed that in working conditions for low clearance, the use of honeycomb adversely affects the leakage flow while it has positive effects for wider Cr sizes. While the honeycomb geometry with a straight tooth reduces the leakage flow by about 11%, this ratio increases to 21.5% with the inclined tooth arrangement.

Keywords: sealing elements; honeycomb seal; inclined labyrinth tooth; sealing CFD.

Reference to this paper should be made as follows: Zengin, İ. and Erdoğan, B. (2023) 'Numerical analysis of geometry and operating conditions in combined honeycomb and inclined labyrinth sealing elements', *Progress in Computational Fluid Dynamics*, Vol. 23, No. 1, pp.1–12.

Biographical notes: İbrahim Zengin is a PhD candidate at the Zonguldak Bülent Ecevit University. He has been also working as a research assistant. His main research interest has been on CFD, turbomachinery, sealing elements, and heat and fluid flow.

Beytullah Erdoğan has been working as an Assistant Professor in the Department of Mechanical Engineering at Zonguldak Bülent Ecevit University. His main research interest has been heat transfer in mini-micro channels and fluid mechanics. He has made also experimental works about his research interest.

1 Introduction

Labyrinth seals are widely used in gas turbines and compressors. Their main task is to prevent gas flow from a high-pressure region to a low-pressure region. Nowadays, labyrinth seals have reached a pretty good point. However, the demands for high efficiency are constantly increasing. Higher pressures and temperatures are required to meet these requirements. Such high operating conditions have led to an increase in the amount of leakage flow through the labyrinth seals in turbomachinery applications. Therefore, the use of labyrinth seals alone is insufficient to meet these demands (Ludwig and Johnson, 1974). When used in combination with different seal models such as labyrinth seal – brush seal, labyrinth seal-honeycomb seal, it positively affects leakage flow (Schramm et al., 2002; Willenborg et al., 2002; Li et al., 2012).

Sealing elements have been developed to increase system efficiency for high-efficiency gas turbines. The development of labyrinth seals has taken almost a century. Many analytical equations (Martin, 1908; Egli, 1935; Hodkinson, 1939; Vermes, 1961; Wolff and Zimmermann, 1987; Childs, 1993) based on the equation proposed by Venant in 1871 emerged for the leakage flow estimation in labyrinth seals. After comparing these equations with the experimental data made subsequently, correction factors were added to the equations. The ESDU technical report summarised these derived equations clearly (ESDU 09004, 2009).

Experimental studies have been carried out to prevent leakage flow from past to present. Ludwig and Johnson (1974) conducted experiments on four different shaft sealing elements. They investigated the gap effect between the fixed stator and the rotor and the thermal behaviour in those regions. They emphasised that increasing leakage flow in aircraft gas turbine engines increases the specific fuel consumption (SFC). It was mentioned that the most critical losses are in the labyrinth seals at the turbine bearing and compressor output. When considering all the calculated losses, these losses cause a 10% decrease in engine power and an increase of 21% in SFC. Stocker (1975) focused on three cases investigating the effect of high-pressure ratio conditions on leakage flow rate, which is a limitation in sealing element designs used in gas turbines. He carried out experiments to visualise the complex behaviour of the flow among the tooth cavities in a water tunnel experiment setup. Using the information obtained from the tests carried out in the water tunnel, he repeated the experiments with airflow both under static and dynamic conditions. In the experiments with water, it was found that the cavities among the teeth tend to produce high levels of turbulence. To obtain the optimum geometry, while examining geometric parameters such as clearance size (Cr), tooth height, and pitch, he also conducted experiments on different pressure ratios and rotor speeds. In geometries in which turbulence increased, he determined a minimum 10% and a maximum 25% decrease in the leakage flow compared to the basic geometry. He emphasised that the effect of rotor speeds on the leakage flow is a slight decrease of 0.0% to 3.2%. Woo (2011) investigated the energy carry-over factors for compressible and incompressible flow conditions in labyrinth seals. For both compressible (air) and incompressible (water) fluids, the energy carry-over factors are the same at $Re \leq 200$, while at $200 \leq Re \leq 500$, the difference between the energy transport factors begins to increase. It was stated that this observed situation is the transition regime. Therefore, the flow regime turns into turbulence even at low Reynolds numbers.

In the last decades, scientists have started to prefer the numerical analysis (CFD) method to predict leakage flow rather than experiments and analytical equations in the literature. Nayak and Dutta (2016a) conducted a study on the windage heating number and the leakage flow performance of honeycomb seals using numerical methods. They emphasised that the honeycomb cells work more actively as Cr size increases and reduce the leakage flow.

The viscous work produced by the rotating components of the sealing elements causes a loss of power and an increase in the total temperature of the fluid. Yan et al. (2009) performed a numerical study on temperature rise and performed CFD analysis on many parameters such as rotor speed, leakage flow rate, clearance size, and pressure ratio. They mentioned that due to the damping property of the honeycomb configuration, the windage heating power is slightly higher than the flat stator surface. They observed approximately 10% more leakage flow in the alone honeycomb geometry case than in the flat stator case. Yan et al. (2012) performed a numerical study to compare the heat transfer and windage heating behaviours of stepped labyrinth seals for flat stator surface and honeycomb stator surface. When they examined the numerical results, they figured out that the differences among the geometries are only in regions with high-temperature. The honeycomb cells have increased the temperature change on the labyrinth tooth surface while significantly reducing the temperature change on the stator surface. When comparing the honeycomb seal stator surface and the flat stator surface, the average heat transfer coefficient at the solid stator surface has decreased by 1/4–1/3 using the honeycomb seal. Therefore, the honeycomb cells have reduced the heat transfer from the hot gas fluid to the solid stator surface.

By the numerical method, Li et al. (2011) compared the effects of the honeycomb cells usage in stepped labyrinth seal on the heat transfer coefficient. They found that the heat transfer coefficient of the honeycomb stator surface under the same operating conditions is approximately three times lower than that of the flat stator surface. They emphasised that the ratio of axial stage length to tooth pitch on heat transfer does not affect both configurations. Willenborg et al. (2002) found that honeycomb placement on opposite surfaces of stepped labyrinth seals acts as additional insulation for the stator surface. They used the LDV method to obtain the velocity distribution of the flow passing through the system. The heat transfer coefficients for both the stator and rotor surfaces were calculated by considering typical motor operating conditions. They found that the Nusselt number is significantly dependent on the clearance size and observed that the Nusselt number increases with increasing clearance size. They also found that honeycomb cells cause a significant decrease in heat transfer on the stator surface. Using optimisation methods, the discharge coefficient performances of the sealing elements are constantly improving. Szymański et al. (2018) stated in their optimisation studies that the most critical factors reducing leakage flow rate are the angle of inclination, thickness, and location of the teeth.

It is understood from the above discussion that studies conducted on the leakage flow rate in sealing elements have focused on analytical prediction, numerical prediction, and experimental measurements. Different designs and combinations have still been investigated to improve sealing performance. However, there are still uncertainties in the effect of honeycomb cell size on leakage flow. The primary purpose of this study is to examine the effects of both honeycomb size and the inclination angle of labyrinth seal, together with their combined cases, on the leakage flow.

2 Material and method

2.1 Description of the problem

Sealing elements control leaks, cooling flows in turbomachinery and contribute to the rotor dynamic stability of the entire system. Sealing elements are exposed to damaging factors such as abrasion, erosion, oxidation,

friction, and residue in thermal, mechanical, aerodynamic, and impact loads. When labyrinth sealing elements in the gas turbine operate at small Cr sizes, the rotor shaft may deviate from the axis of rotation. At the same time, an increase in fluid velocity may occur due to sudden throttling. This situation reveals frictions between the labyrinth tooth tip-stator surfaces. Therefore, variable conditions such as the rotor axis deviation and sudden pressure changes during take-off, cruise, and landing make the tooth tip friction and flow friction inevitable. Surface friction causes an increase in solid surface temperature and brings along the surface abrasion of the material, the expansion of the material. Variable operating conditions mean that the position of the teeth in the radial direction will constantly change. During the radial movement, friction-induced abrasions occur between the labyrinth tooth and the stator surface. These abrasions negatively affect the leakage flow rate because of increasing the passage area of the flow. Each vortex in the labyrinth seal causes the flow to lose its pressure energy and positively affects the leakage flow. Therefore, the honeycomb seals' damping feature is utilised, and also it increases the vortices inside the sealing element. As seen in Figure 1, working fluid enters the airflow area from the inlet boundary area, gradually loses its pressure energy in each tooth, and leaves the exit boundary area where the static pressure is present after the last tooth.

Figure 1 Schematic of the problem (see online version for colours)

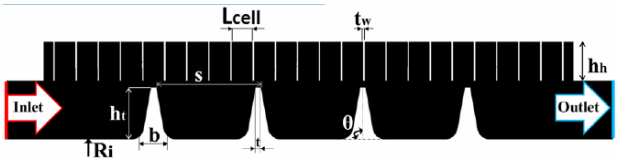

The seal geometry was designed for the present study considering dimensions widely used in the literature and industry. The geometric dimensions and parameters examined are shown in detail in Table 1.

2.2 Analytical approach

As discussed in the introduction, many equations have been derived to predict leakage flow in the literature. Table 2 contains the equations determining the leakage flow for straight labyrinth seals along the axis. The authors specifically selected the equations by considering compressible flow conditions. There are two coefficients in Table 2 that include the effect of the energy transfer factor (carry-over factor, k) and the impact of discharge coefficient (Cd) into the equations. When deriving the ideal equations, it is assumed that all the pressure energy is lost by expanding in the cavities, and the kinetic energy is zero at the entrance of the next tooth. Some pressure energy expands, and the remainder attacks the entrance of the next tooth at an increasing speed with the effect of constriction in the previous tooth. To account for this effect, a factor coefficient called the energy transfer rate (k) is used. The discharge coefficient (Cd) is used to model the impact of throttling on the flow path. The flow will be separated from the sharp entrance edge except where very low Reynolds number and compressibility effects are important.

Table 1 Constant and varying parameters

Varying parameters		*Symbol*	*Values*
1	Honeycomb cell sizes, mm (in)	Lcell	0.793 (1/32"), 1.590 (1/16"), 3.175 (1/8")
2	Clearance, mm	Cr	0.254, 0.508, 1.016
3	Tooth inclination angles, degree	θ	90, 70, 50
4	Pressure ratio	π	1.5; 2.0; 2.5
5	Rotor speed, m/s	Vr	0; 200; 400
Constant parameters		*Symbol*	*Values*
1	Tooth pitch, mm	s	8
2	Tooth height, mm	h_t	4
3	Tooth base width, mm	B	1.811
4	Tooth tip width, mm	T	0.4
5	Honeycomb wall thickness, mm	t_w	0.102
6	Honeycomb height, mm	h_h	3
7	Rotor tooth base radius, mm	Ri	253

Consequently, this separation will cause a reduction in the effective flow field. This effect is modelled through the discharge coefficient. Zimmermann and Wolff (1998) reported the Cd coefficient graphs. CFD analysis for flat stator and axial straight labyrinth seals are compared using the appropriate coefficients in the equations discussed above.

2.2.1 Discharge coefficient (Cd)

When fluid flows pass through the throttling zone, there is a decrease in the net cross-sectional area through which the fluid passes. Especially for compressible flows, this area reduction becomes more critical due to sudden density changes. Therefore, calculating the mass flow rate in throttling flows usually needs the discharge coefficient. The discharge coefficient represents the ratio of the actual flow amount to the flow amount that should theoretically pass and is calculated by equation (1).

$$Cd = \frac{\dot{m}_{actual}}{\dot{m}_{theoric}} \tag{1}$$

The mass flow rate through a nozzle with the theoretical isentropic flow assumption can be calculated by equation (2).

$$\dot{m}_{theoric} = \frac{P_{t0} A}{\sqrt{T_{t0}}} \sqrt{\frac{2\gamma}{R(\gamma-1)} \left[\left(\frac{1}{\pi}\right)^{2/\gamma} - \left(\frac{1}{\pi}\right)^{\gamma+1/\gamma} \right]} \tag{2}$$

π shows the pressure ratio between the total pressure ratio at the inlet and the static pressure at the outlet. Expression A

represents the cross-sectional area through which the flow passes at the minimum clearance size between the rotor tooth and the stator. Equation (2) also applies to unchoked flows. As the pressure ratio (π) increases, the mass flow rate in the equation tends to increase. However, if the pressure ratio is above the critical ratio, the mass flow rate approaches the throttling point, and the mass flow rate remains constant. The critical pressure ratio is:

$$\left(\frac{1}{\pi}\right)_{cr} = \left(\frac{2}{\gamma+1}\right)^{\gamma/\gamma+1} = 0.5282 \tag{3}$$

It is well-known to determine the amount of leakage flow occurring in straight labyrinth seals without using a honeycomb seal using the theoretical flow rate and the discharge coefficient. However, it is necessary to represent the effect of using a honeycomb seal on the amount of leakage flow with a coefficient. This coefficient is defined by equation (4).

$$\zeta = \frac{Cd_{HC}}{Cd_{FS}} \tag{4}$$

Here, *FS* represents the discharge coefficient for the flat stator case, while *HC* represents the discharge coefficient for the honeycomb use case. The cross-sectional flow areas used in the theoretical flow calculation for both cases represent the annulus area in the clearance (Cr) region. This coefficient measures the comparison according to the flat stator situation. If it is below one, using the honeycomb seal positively affects the leakage flow. The graphics show the calculations with the coefficient of discharge (*Cd*) and the effective coefficient of using the honeycomb seal (ζ).

2.3 Numerical modelling

To model the turbulent flow in honeycomb and labyrinth seal elements, Navier-Stokes, and energy equations should be solved numerically, as seen in equations (5), (6) and (7). The necessary NS equations are solved with ANSYS – Fluent, which uses the finite volume method. Modelling both 3D and 360° of flow geometry requires high mesh density and long computational time. Therefore, the analyses were carried out over a periodic part of the flow volume, as shown in Figure 2. Total pressure and temperature are defined at the inlet boundary condition, while 1 atm is defined as the static pressure at the outlet boundary condition. Fixed wall surfaces were defined as non-slip conditions, while translational velocity condition was defined for rotor surfaces. Wall surfaces were also defined as adiabatic. The side surfaces of the flow volume were defined as the translational periodical boundary conditions. The iteration steps were continued until the continuity, velocity, energy, and turbulence error residues for the x-y-z directions were 10^{-6}. Governing equations are as follows, respectively (Ansys Inc, 2013):

$$\frac{\partial \rho}{\partial t} + \nabla \cdot \left(\rho \vec{V}\right) = S_m \tag{5}$$

$$\frac{\partial \left(\rho \vec{V}\right)}{\partial t} + \nabla \cdot \left(\rho \vec{V}\vec{V}\right) = -\nabla p + \rho \vec{g} + \vec{F} \tag{6}$$

$$\frac{\partial (\rho E)}{\partial t} + \nabla \cdot \left(\vec{V}(\rho E + p)\right) = -\nabla \cdot \left(\sum\nolimits_j h_j J_j\right) + S_h \tag{7}$$

For the selection of the appropriate turbulence model and intensity, the authors preferred models predicting the flow physics accurately in labyrinth seals and honeycomb seals within the scope of the literature (Desando et al., 2015a, 2015b; Fraczek et al., 2016; Nayak and Dutta, 2016a, 2016b; Yan et al., 2018; Wroblewski and Bochon, 2015). In this study, calculations were performed with the realisable *k-ε* turbulence transport model with two equations, which was accepted by the literature and compatible with the experimental results. The equations are shown in equations (4)–(5). Turbulence intensity has been chosen as 5% both for the inlet and outlet boundary.

$$\frac{\partial (\rho k)}{\partial t} + \frac{\partial \left(\rho k u_j\right)}{\partial x_j} = \frac{\partial}{\partial x_j}\left[\left(\mu + \frac{\mu_t}{\sigma_k}\right)\frac{\partial k}{\partial x_j}\right] + G_k + G_b - \rho\varepsilon - Y_M + S_k \tag{8}$$

$$\frac{\partial (\rho \varepsilon)}{\partial t} + \frac{\partial \left(\rho \varepsilon u_j\right)}{\partial x_j} = \frac{\partial}{\partial x_j}\left[\left(\mu + \frac{\mu_t}{\sigma_k}\right)\frac{\partial \varepsilon}{\partial x_j}\right] + \rho C_1 S_\varepsilon - \rho C_2 \frac{\varepsilon^2}{k + \sqrt{\nu\varepsilon}} + C_{1\varepsilon}\frac{\varepsilon}{k} C_{3\varepsilon} G_b + S_\varepsilon \tag{9}$$

k, ε in equations (8) and (9) indicate respectively the turbulence kinetic energy and its dissipation rate. The turbulent viscosity term (μ_t) shown in the equation is calculated by equation (10). G_k, G_b, and Y_M represent respectively turbulent kinetic energy production resulting from average velocity gradients, turbulent kinetic energy production due to buoyancy, the contribution of fluctuating dilatation at compressible turbulence to the overall dissipation rate. S_k and S_ε are user-defined resource terms. σ_k and σ_ε are the turbulence Prandtl constant for *k-ε*, model constants C_2 and $C_{1\varepsilon}$ are given in equation (11).

$$\mu_t = \rho C_\mu \frac{k^2}{\varepsilon} \tag{10}$$

$$C_{1\varepsilon} = 1.44,\ C_2 = 1.9,\ \sigma_k = 1.0,\ \sigma_\varepsilon = 1.2 \tag{11}$$

The thermal conductivity (k = 0.02514 W⁄m.K), specific heat (Cp = 1007 J⁄kg.K), and viscosity (μ = 1.825 × 10^{-5} kg⁄m.s) of the air inside the labyrinth seal were considered as constant under the inlet air temperature conditions (293 K). But the density (ρ) of the air was calculated with the ideal gas equation. More data on flow characteristics are given in Table 3.

Table 2 Analytical equations in literature

Equation's name	k_{factor} – *(carry-over factor)*	*Equation*
Martin equation	-	$\dot{m} = AP_{t0}\sqrt{\frac{1-(P_n/P_{t0})^2}{RT_{t0}\left[n-\ln(P_n/P_{t0})\right]}}$
Hodkinson equation	$k_h = \sqrt{\frac{1}{1-\frac{n-1}{n}\cdot\frac{(s/t)}{(s/t)+0.02}}}$	$\dot{m} = k_h AP_{t0}\sqrt{\frac{1-(P_n/P_{t0})^2}{RT_{t0}\left[n-\ln(P_n/P_{t0})\right]}}$
Vermes equation	$k_v = \sqrt{\frac{1}{1-\frac{8.52}{(s/t)/t+7.23}}}$	$\dot{m} = C_d k_v AP_{t0}\sqrt{\frac{1-(P_n/P_{t0})^2}{RT_{t0}\left[n-\ln(P_n/P_{t0})\right]}}$
Zimmermann and Wolff equation	$k_z = \sqrt{\frac{\frac{n}{n-1}}{1-\frac{n}{n-1}\cdot\frac{(s/t)}{(s/t)+0.02}}}$	$\dot{m} = C_d k_z AP_{t0}\sqrt{\frac{1-(P_n/P_{t0})^2}{RT_{t0}\left[n-\ln(P_n/P_{t0})\right]}}$
Orifice approach	-	$\dot{m} = AP_{t0}\sqrt{\frac{2\gamma}{RT_{t0}(\gamma-1)}\left[\left(\frac{P_{i+1}}{P_i}\right)^{2/\gamma}-\left(\frac{P_{i+1}}{P_i}\right)^{(\gamma+1)\gamma}\right]}$

Figure 2 Numerical model and boundary conditions (see online version for colours)

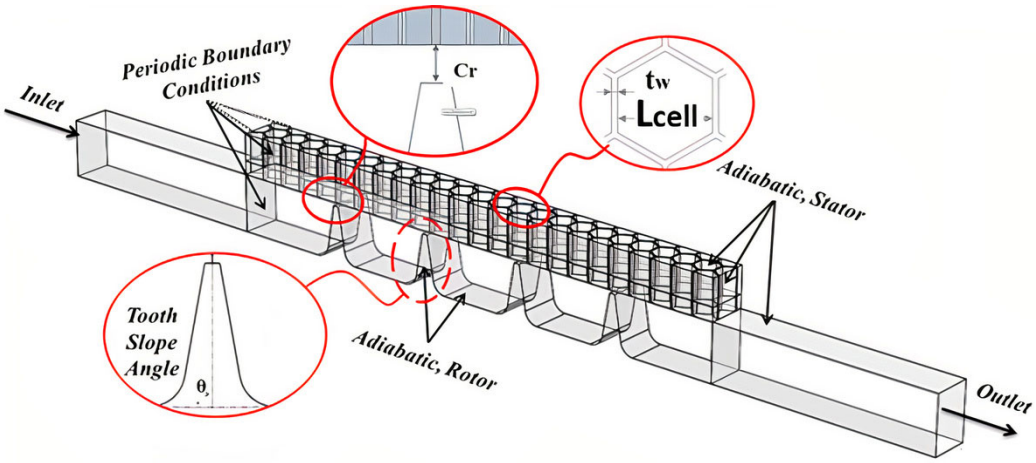

Table 3 Flow properties

Fluid	*Air, ideal gas*
Regime	Steady state
Flow model	Turbulence flow model: *k-ε*/realisable wall function: enhanced wall treatment
Discretisation method	Second order upwind
Geometry model	Periodic slice

The optimum number of mesh elements was determined by gradually increasing the number of meshes for three-dimensional periodic flow geometry with mesh independence analysis. Table 4 shows mesh independence analysis for the smallest honeycomb cell size (1/8"–0.793 mm) and Cr size (0.127 mm) representatively. It was determined that the mass flow rate does not change after approximately two million elements for flow volumes created according to geometric parameters.

Table 4 Mesh independence analysis

Number of elements	*Number of nodes*	*Leakage flow rate [g/s]*
686,038	849,653	42.09
1,115,624	1,340,612	33.00
1,418,026	1,678,989	32.41
2,010,204	2,341,211	32.30
2,199,916	2,546,639	32.28
2,489,000	2,873,809	32.21

Figure 3 shows the representative mesh elements view for the flow field. The denser mesh was carried out in contraction and near-wall regions where the flow gradients change. The enhanced wall treatment function accurately captured the flow physics in the near-wall regions. For this wall function, the y^+ value should be approximately 1. The y^+ value varies between 2 and 3 in the movable (rotor) and fixed (honeycomb and stator) wall regions.

A non-conformal mesh interface was used to communicate separate geometries created for honeycomb and labyrinth seals. With the creation of two separate seals as a whole domain, some problems have arisen in mesh and converge issues. The authors took care of these problems with the non-conformal mesh interface.

Figure 3 (a) Representative mesh view for honeycombs (b) Constricted region (see online version for colours)

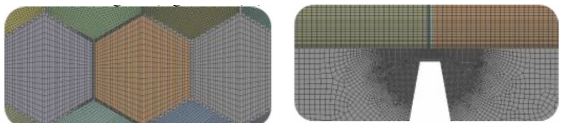

(a) (b)

3 Results and discussion

The authors studied honeycomb and labyrinth seal elements in a wide parameter range in this study. The study focused on four different geometric cases. After verifying the first three cases with literature comparisons, case 4 geometry parameters, the main subject of the study, were examined in detail.

- Case 1: flat stator – axial straight tooth labyrinth seal.
- Case 2: flat stator – inclined (70-50 degrees) tooth labyrinth seal.
- Case 3: honeycomb placement stator – axial straight tooth labyrinth.
- Case 4: honeycomb placement stator – inclined tooth labyrinth seal. The investigated geometric variations are given in Figure 4.

Figure 4 Investigated geometric variations

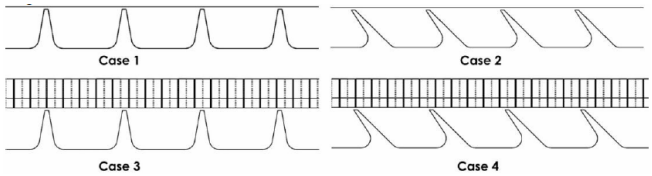

While comparing case 1 with the well-known analytical equation in the literature, case 2 and case 3 were compared to the results obtained from Stocker's experimental data in ref. (Stocker et al., 1977). As shown in Figure 5, CFD results with equations for flat stator and axial straight labyrinth tooth are in good agreement. The maximum error rates among the equations and CFD results were calculated as 28.2% for Martin, 20.8% for Hodkinson, 4.7% for Zimmermann and Wolff, 25% for the Orifice approach, and 24.2% for the Vermes equation, respectively. Zimmermann and Wolff's equation is the analytical equation that best fits with CFD results. As expected, the maximum error rate is in the Martin equation because the Martin equation is the first derived equation, and the correction coefficients are not included in his equation.

Figure 5 Results for flat stator and axial straight tooth (case 1), $\pi = 1.5$

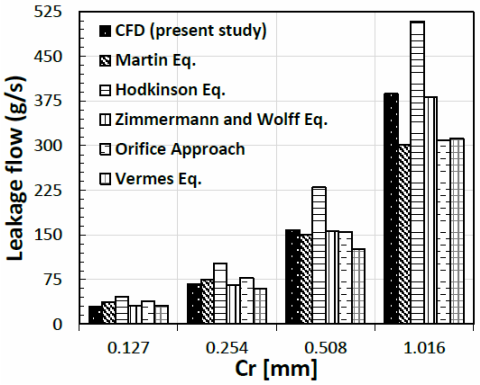

For case 1, experimental results for the stepped tooth labyrinth seal mentioned in ref. (Schramm et al., 2002) were used to validate the turbulence model and discretisation method used in the numerical analysis. The y+ value on the wall surfaces was around 1.14 in the mesh structure created for the stepped labyrinth seal. The *k-ε* realisable/enhanced wall treatment wall function was used, and the discretisation of the equations was done by the second-order upwind. The PRESTO approach was used to connect the pressure and velocity couple. It was determined that the turbulence model used was in good agreement with the experimental data. These comparison results are mentioned in Figure 6 and Figure 7.

Figure 6 Experimental and CFD results for flat stator and axial stepped labyrinth tooth

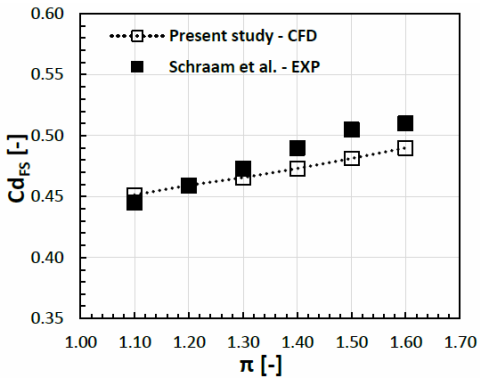

Stocker's experimental data were used to compare the flat stator and inclined tooth analysis. Stocker carried out experiments at 90°, 70°, and 50° of inclination angles with limited clearance sizes. Although Stocker's working conditions and basic labyrinth seal geometry dimensions are different from this study, the effect of tooth inclination angles on the leakage flow rate has shown a similar decrease as seen in Table 5. It also includes the error rates. The main differences between test data and CFD results are different working conditions such as tooth pitch distance, tooth angle, tooth tip width, tooth height, tooth number, and assumptions made in the analyses. However, the effects of tooth inclination angles on the leakage flow have shown similar reduction rates.

Figure 7 Flow field comparison, stepped labyrinth – flat stator configuration, π = 1.1, (a) Schraam et al. – experimental and CFD velocity vectors, (b) present study – CFD velocity vectors (see online version for colours)

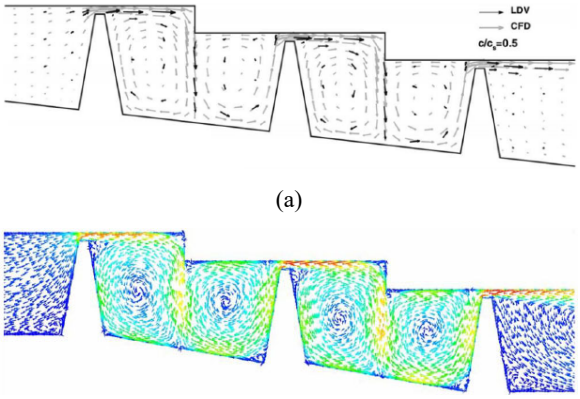

(a)

(b)

Table 5 Analysis results for flat stator and inclined teeth (case 2)

Cr [mm]	*Inclination angle [°]*	*Leakage flow rate reduction (%)***		
		CFD	*Stocker's exp.*	*Error rate*
0.127	70	~4.18%	-	-
	50	~4.15%	-	-
0.254	70	~5.5%	~5%	10%
	50	~6.76%	~7%	3.4%
0.508	70	~6.1%	~9%	32.2%
	50	~9%	~12%	25%
1.016	70	~3.15%	-	-
	50	~6.55%	-	-

Note: **Percentage changes were calculated according to the 90° tooth angle.

Another comparison analysis is for case 3, which is both straight labyrinth teeth and honeycomb placement. It was determined that as clearance size increases, using honeycomb sealing elements on the stator surface results in less leakage flow in the system. The effect of honeycomb cell use on leakage flow rate has been shown by CFD analysis results (present study) and Stocker's experimental data (π = 2.0) in Figure 8. Stocker interpreted the effect of honeycomb cell use similarly in his study in ref. (Stocker et al., 1977). Small honeycomb cell sizes should be preferred for situations where the clearance sizes are very small, but the opposite is the case for large clearance sizes. It can be stated that the honeycomb effect coefficient (ζ) is below one for values greater than about 0.2 of the Cr/Lcell ratio and the use of honeycomb has a positive effect on the leakage flow. This complex situation has been given in Figure 9 for π = 1.5, Cr = 0.127, and Cr = 1.016 mm. When honeycomb cells are used at large Cr sizes, the vortex formation inside the honeycomb cells is more than the vortex formation at small Cr sizes. These eddies absorb the pressure energy of the flow, causing a significant reduction in the leakage flow. For Cr = 0.254-0.508-1.016 mm, this resulted in a decrease of approximately 6.7%, 11.7%, and 28.7% in the amount of leakage flow, respectively. It is well-known that if both labyrinth and honeycomb seals are used, it positively affects leakage flow. However, choosing the appropriate honeycomb size reveals the importance of this issue.

For the fourth case, evaluations were made on the honeycomb effect coefficient (ζ). CD_{FS} in equation (4) represents a straight stator 90° tooth angle and a flat stator. Equation (4) makes the effect of both honeycomb and tooth inclination angle better interpretable. Since the use of honeycomb at the smallest Cr size (0.127 mm) did not have a positive effect, the evaluation was carried out for three different Cr sizes.

The honeycomb effect coefficient (ζ) is below one for all angles when using the smallest honeycomb (0.793 mm). At the same time, the best leakage flow reduction for Cr = 0.254 and 0.508 mm occurred at the 70° tooth angle with 8.2% and 16.02%, respectively, while the best leakage flow reduction for Cr = 1.016 mm occurred at the 50° tooth angle with 15.6%. Figure 10 shows the effect of tooth inclination for 0.793 mm of the honeycomb size.

The honeycomb effect coefficient (ζ) is below one for all angles for Cr = 0.508 and 1.016 mm when using 1.590 mm of the honeycomb size. But above one for Cr = 0.254 mm for all angles. For Cr = 0.508 and 1.016 mm, the best leakage flow reduction occurred at 50° tooth inclination angle with 21.2% and 19.7%, respectively. Figure 11 shows the effect of tooth inclination for 1.590 mm of the honeycomb size.

The honeycomb effect coefficient (ζ) is about one and above for Cr = 0.254 and 0.508 mm when using 3.175 mm of the honeycomb size, while the honeycomb effect coefficient (ζ) for Cr = 1.016 mm is below one. However, a positive effect of the inclination of the labyrinth teeth on the leakage flow was not detected for Cr = 1.016 mm. The best leakage flow reduction occurred with 28.7% at a 90° inclined tooth angle. Figure 12 shows the effect of tooth inclination for 1.590 mm of the honeycomb size.

The Mach number and pressure contours are shown in Figure 13. As can be seen from the Mach number contours on the honeycomb surfaces, the Mach number reaches the maximum level on the honeycomb surface at an inclination angle of 50°. It also reveals the increase in pressure loss. It was determined that eddies in the honeycomb cells cause a decrease in leakage flow by absorbing the pressure energy of the flow due to friction on the honeycomb walls. At a 50° inclined tooth angle, the pressure distribution decreases more gradually than other tooth angles. However, the last tooth has experienced a greater pressure drop than other tooth angles.

Figure 8 The use of honeycomb with straight tooth and its leakage flow behaviour (case 3)

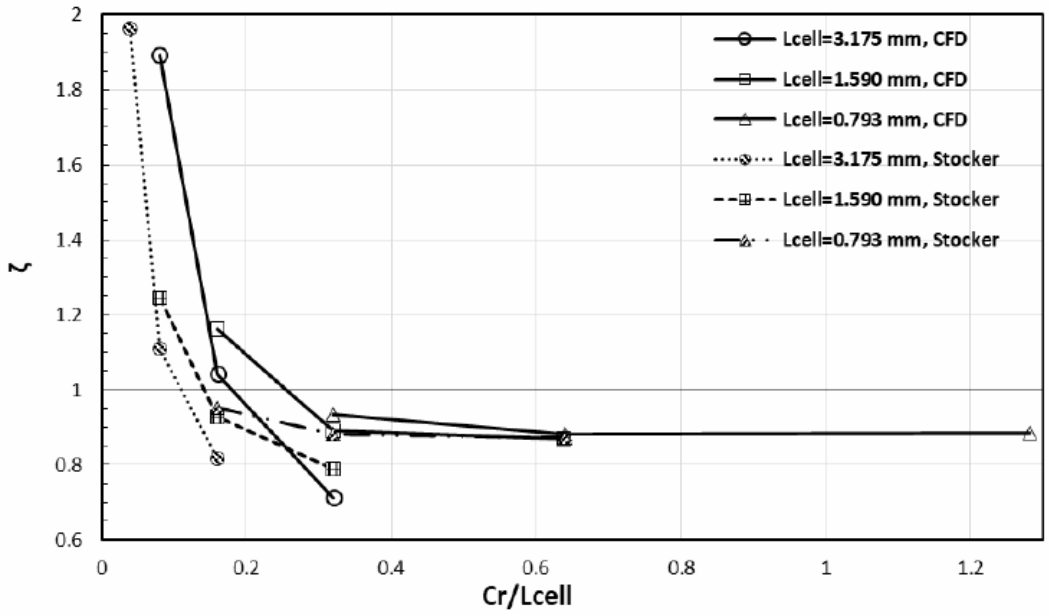

Figure 9 Mach number contours for Cr = 0.127 mm on the left-view, Cr = 1.016 mm on the right-view (case 3), π = 1.5 (see online version for colours)

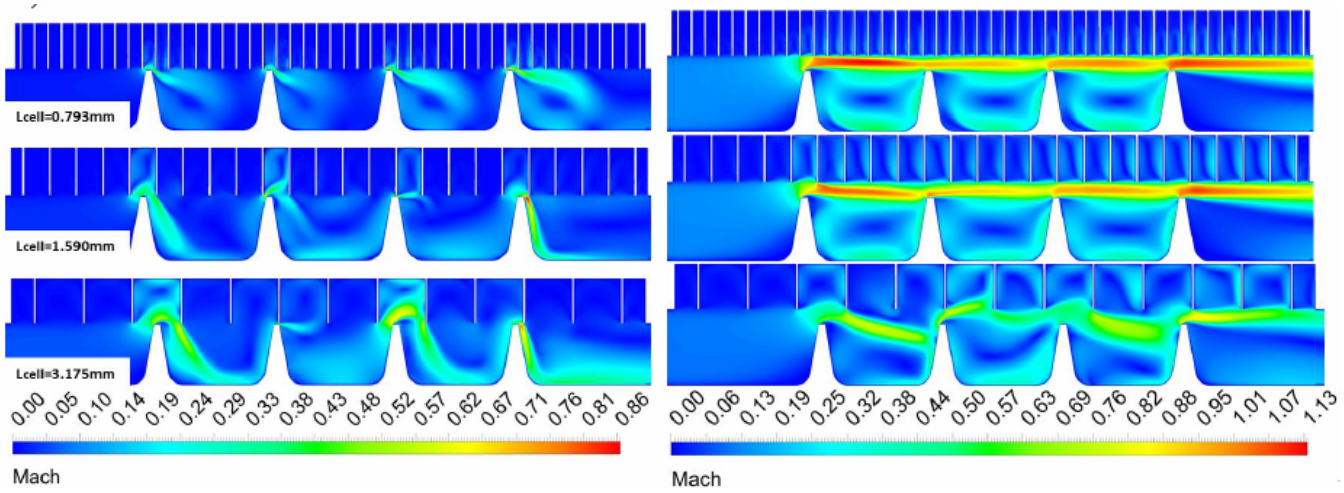

Figure 10 The effect of tooth inclination for 0.793 mm of the honeycomb size, π = 1.5

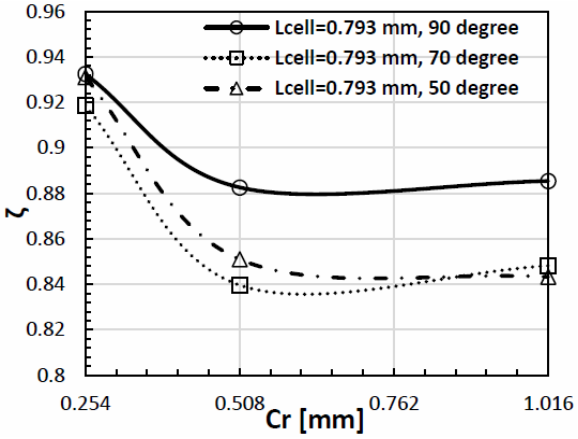

Figure 11 The effect of tooth inclination for 1.590 mm of the honeycomb size, π = 1.5

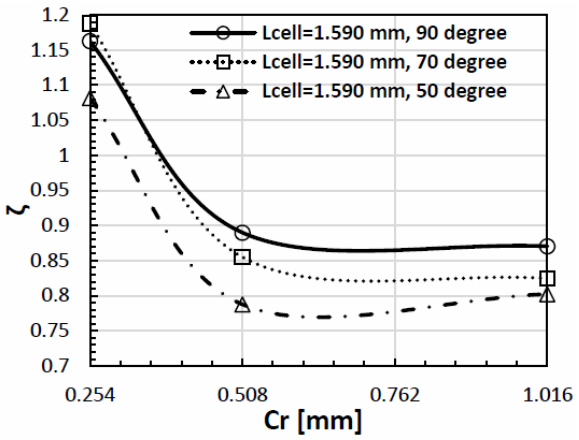

Figure 12 The effect of tooth inclination for 3.175 mm of the honeycomb size, π = 1.5

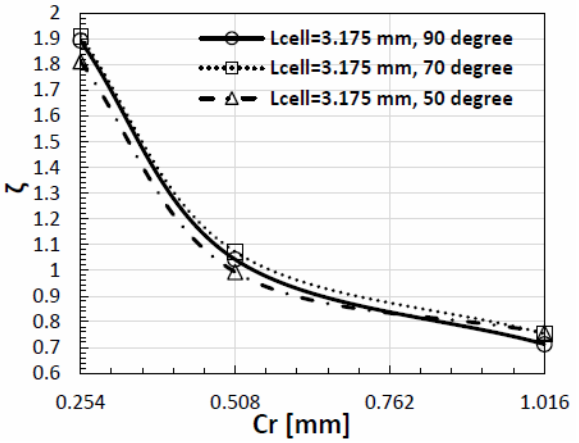

Figure 13 (a) Mach number contours and (b) Pressure contours, for Lcell = 1.590 and Cr = 0.508 mm, π = 1.5 (see online version for colours)

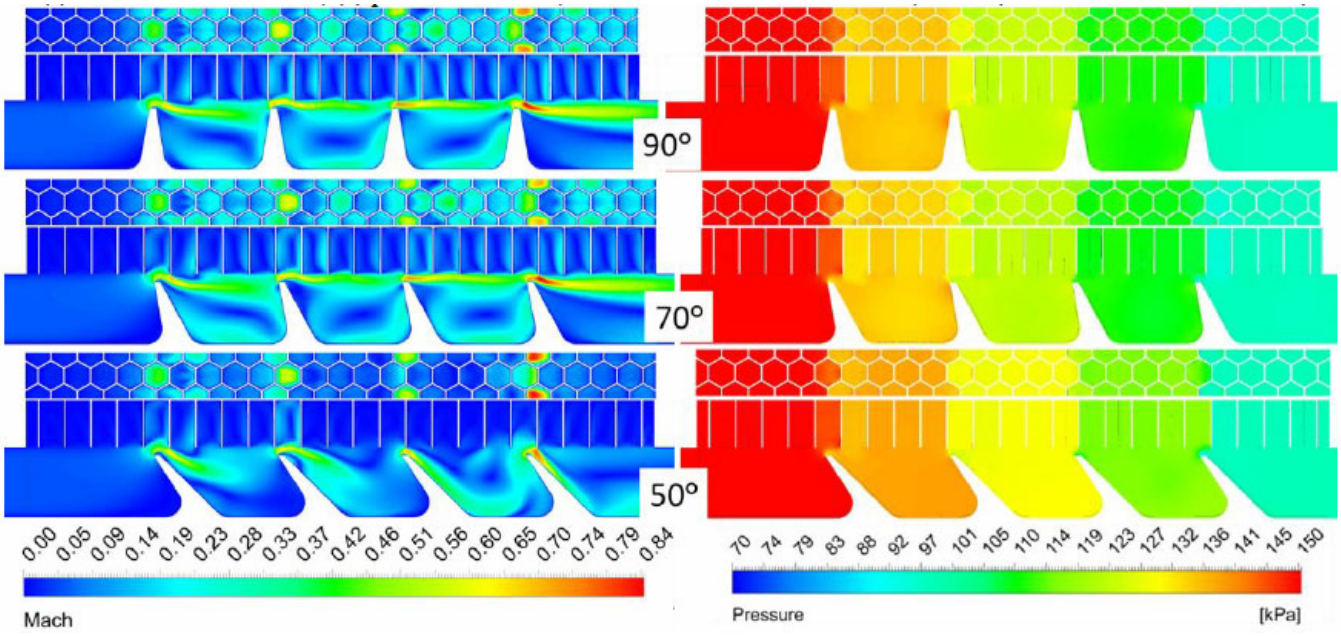

(a) (b)

Figure 14 The effects of (a) pressure, Vr = 0 and (b) rotor speed, π = 1.5 as operating conditions on leakage flow

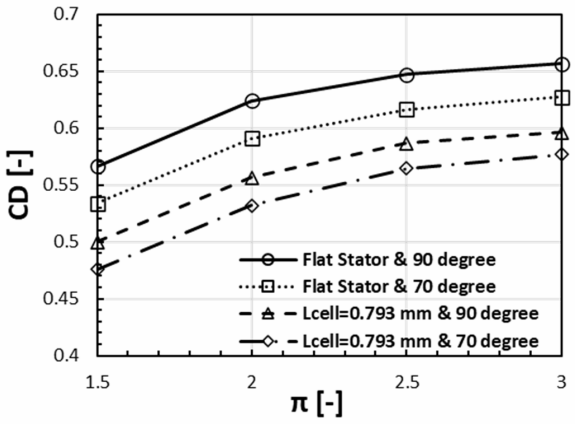

(a)

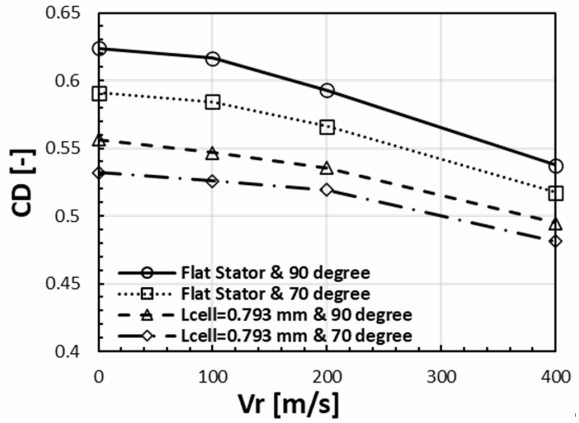

(b)

In addition to the geometric parameters, another critical parameter affecting the leakage flow is the engine operating conditions. This study examines the pressure ratio and the rotor speeds as engine operating conditions. As shown in Figure 14(a), the leakage flow rate increases as the pressure ratio ($P_{t,inlet}/P_{n,outlet}$) increases from 1.5 to 2.0, an increase in leakage flow of approximately 53% is observed. When increasing the pressure ratio from 2.5 to 3.0, an increase in leakage flow of roughly 21% is observed. It is understood that as the pressure ratio inside the sealing element increases, the flow converges towards the choking point. Gas turbines operate at variable shaft speeds depending on the load. Higher rotor speeds can change the regime of flow through the labyrinth seal. Therefore, circumferential velocity vectors in the flow due to rotor speeds force the flow along the shaft axis to change its direction. This flow behaviour increases the vortex effect through the labyrinth seal and causes a decrease in the leakage flow rate. Figure 14(b) shows the effect of rotor speeds on leakage flow. There may be a sudden decrease in the leakage flow at a high velocity where circumferential velocities are dominant.

4 Conclusions

This study covers the investigation of quite wide parameters on understanding labyrinth seal and honeycomb seal flow characteristics. Firstly, CFD analyses for flat stator and straight tooth labyrinth seal (case 1) were compared with well-known equations proven in the literature. At the same time, the turbulence model used in the present study was confirmed by the experimental study data available in the literature. Then, CFD analyses were performed to examine the effect of honeycomb use (case 3) and the impact of tooth inclination angle (case 2) separately, and numerical results were compared with the experimental data as possible. Finally, case 4 was comprehensively studied in terms of geometric sizes and operating conditions. The main results obtained from the study can be summarised as follows:

- CFD analysis results at low clearance sizes are in good agreement with both analytical and experimental data.
- Zimmermann's equation fits best with CFD analysis results for straight stator – straight tooth (case 1).
- For the flat stator surface, the maximum reduction in leakage flow through the labyrinth seal has occurred at.
- 50° tooth angle. However, the amount of reduction in leakage flow varies significantly according to the Cr sizes.
- The effect of honeycomb seal and straight tooth labyrinth seal use (case 3) has been studied in detail. While the use of honeycomb for small Cr sizes increases the leakage flow and hence discharge coefficient, this flow behaviour shows the opposite effect for large Cr sizes. The honeycombs work more actively as the Cr size increases and the swirl efficiency increases. Therefore, the discharge coefficient has decreased significantly. Both Cr and honeycomb sizes are effective on leakage flow. As shown in Figure 8, when the Cr/Lcell ratio is greater than approximately 0.2, the honeycomb effect coefficient comes down below one. Above this rate, the amount of leakage flow decreases significantly.
- When used honeycomb seal and inclined tooth labyrinth seal (case 4), the reduction rate in the leakage flow rate has improved significantly. Using small-size honeycomb seals in working conditions with small Cr sizes seems advantageous. The inclined labyrinth teeth have shown the best effect at the honeycomb size of 1.590 mm and the Cr size of 0.508 mm. While the best leakage flow reduction ratio in these dimensions is at 21.2% to 50° tooth inclination angle, it was determined that the inclined labyrinth teeth do not have much effect in using a large honeycomb size.
- It was observed that the increase in the pressure ratio significantly increases the leakage flow, but this increase in leakage flow decreases as the throttling point converges.

- The study investigated the effect of four different rotor speeds on leakage flow. As the rotor shaft speed increases, the leakage flow rate decreases through the labyrinth seal. The vital reason for the decrease of the leakage flow is that the rotor speed forces the direction of the fluid flow towards the direction of rotor rotation. Leakage flow has decreased significantly after the critical rotation speed of 200 m/s.
- Honeycomb seals are generally preferred to prevent excessive wear and thermal problems caused by hot gas. It is considered that choosing honeycomb placement – inclined tooth (case 4) in regions where leakage flow rates and wear probability is high will be beneficial in terms of system operating life and price performance.

Acknowledgements

Financial support for this study was provided by Zonguldak Bülent Ecevit University-Scientific Research Project (Project Code No. 2018-77654622-02). The authors gratefully acknowledge the institution for their support.

References

Ansys Inc. (2013) *ANSYS Fluent Theory Guide*, Ansys, Inc., Canonsburg, PA, p.814.

Childs, D.W. (1993) *Turbomachinery Rotordynamics Phenomena, Modeling and Analysis*, First ed., p.430, John Wiley & Sons, New York.

Desando, A., Rapisarda, A., Campagnoli, E. and Taurino, R. (2015a) *Numerical Analysis of Honeycomb Labyrinth Seals: Cell Geometry And Fin Tip Thickness Impact on the Discharge Coefficient*, American Society of Mechanical Engineer GT2015-42106, Montreal-Canada, pp.1–11.

Desando, A., Rapisarda, A., Campagnoli, E. and Taurino, R. (2015b) 'Rounded fin edge and step position effects on discharge coefficient in rotating labyrinth seals', *Journal of Turbomachinery*, Vol. 138, No. 1, pp.1–17.

Egli, A. (1935) 'The leakage of steam through labyrinth seals', *Transactions of the ASME*, Vol. 57, pp.115–122.

ESDU 09004 (2009) *Labyrinth Seal Flow*, ISBN: 978 1 86246 639 5.

Fraczek, D., Bochon, K. and Wroblewski, W. (2016) 'Influence of honeycomb land geometry on seal performance', *ASME Conference GT2016-57569*, Seoul-South Korea, pp.1–11.

Hodkinson, B. (1939) 'Estimation of leakage through a labyrinth gland', *Proceedings of the Institute of Mechanical Engineers*, Vol. 141, pp.283–288.

Li, J., Qiu, B., Jiang, S., Kong, X. and Feng, Z. (2012) 'Experimental and numerical investigations on the leakage flow characteristics of the labyrinth brush seal', *Journal of Engineering for Gas Turbines and Power*, Vol. 134, No. 10, pp.1–9.

Li, J., Yan, X. and Feng, Z. (2011) 'Effects of sealing clearance and stepped geometries on discharge and heat transfer characteristics of stepped labyrinth seals', *Part A: Journal Power and Energy*, Vol. 225, No. 4, pp.521–537.

Ludwig, L.P. and Johnson, R.L. (1974) *Sealing Tecnology for Aircraft Gas Turbine Engines*, NASA-TM-X-71607, The Technical Paper, California, pp.1–7.

Martin, H. (1908) 'Labyrinth packings', *The Engineer*, Vol. 85, pp.35–38.

Nayak, K.C. and Dutta, P. (2016a) 'Numerical investigations for leakage and windage heating in straight – through labyrinth seals', *Journal of Engineering for Gas Turbines and Power*, Vol. 138, No. 1, pp.1–10.

Nayak, K.C. and Dutta, P. (2016b) 'Effect of rub-grooves on leakage and windage heating in straight-through labyrinth seals', *Journal of Tribology*, Vol. 138, No. 022201, pp.1–11.

Schramm, V., Willenborg, K., Kim, S. and Wittig, S. (2002) 'Influence of a honeycomb facing on the flow through a stepped labyrinth seal', *Journal of Engineering for Gas Turbines and Power*, Vol. 124, No. 1, pp.140–146.

Stocker, H.L. (1975) 'Advanced labyrinth seal design performance for high pressure ratio gas turbines', *American Society of Mechanical Engineer: Winter Annual Meeting*, Texas, pp.1–11.

Stocker, H.L., Cox, D.M. and Holle, G.F. (1977) *Aerodynamic Performance of Conventional and Advanced Labyrinth Seals with Solid-Smooth, Abradable and Honeycomb Lands*, NASA/CR-135307, Indiana.

Szymański, A., Wróblewski, W., Frączek, D., Bochon, K., Dykas, S. and Marugi, K. (2018) 'Optimization of the straight-through labyrinth seal with a smooth land', *ASME J. Eng. Gas Turbines Power*, Vol. 140, No. 12, p.122503.

Vermes, G. (1961) 'A fluid mechanics approach to labyrinth seal leakage problem', *Journal of Basic Engineering*, Vol. 83, No. 2, pp.161–169.

Willenborg, K., Schramm, V., Kim, S. and Wittig, S. (2002) 'Influence of a honeycomb facing on the heat transfer in a stepped labyrinth seal', *Journal of Engineering for Gas Turbines and Power*, Vol. 124, No. 1, pp.133–139.

Wolff, K.H. and Zimmerman, H. (1987) *Comparison between Empirical and Numerical Labyrinth Flow Correlations*, American Society of Mechanical Engineer, New York, pp.1–6.

Woo, J.W. (2011) *Analysis of Compressible and Incompressible Flows*, Master thesis, Yonsei University, Korea, 150s.

Wroblewski, W. and Bochon, K. (2015) 'Conjugate heat transfer analysis of the tip seal in the counter rotating low pressure turbine', *Institute of Power Engineering and Turbomachinery*, Vol. 67, No. 3, pp.253–270.

Yan, X., Dai, X., Zhang, K., Li, J. and He, K. (2018) 'Effect of teeth bending and mushrooming damages on leakage performance of a labyrinth seal', *Journal of Mechanical Science and Technology*, Vol. 32, No. 10, pp.4697–4709.

Yan, X., Li, J., He, K. and Feng, Z. (2012) 'Investigations of the conjugate heat transfer and windage effect in stepped labyrinth seals', *International Journal of Heat and Mass Transfer*, Vol. 15, Nos. 17–18, pp.4536–4547.

Yan, X., Li, J., Song, L. and Feng, Z. (2009) 'Investigations on the discharge and total temperature increase characteristics of the labyrinth seals with honeycomb and smooth lands', *Journal of Turbomachinery*, Vol. 131, No. 4, pp.1–8.

Zimmermann, H. and Wolff, K.H. (1998) *Air System Correlations/Part 1: Labyrinth Seals*', American Society of Mechanical Engineer 98-GT-206, New York, pp.1–8.

Nomenclature

A	Clearance flow area
b	Tooth base width
Cr	Clearance between stator and tooth tip
Cd	Discharge coefficient
E	Total energy
$\vec{F}$	External force vector
$\vec{g}$	Gravitational vector
G_k	Generation of turbulent kinetic energy due to the mean velocity gradients
G_b	Generation of turbulent kinetic energy due to buoyancy
h_h	Honeycomb cell height
h_t	Tooth height
h_i	Sensible enthalpy of j component
J_i	Diffusion flux of j component
k	Turbulent kinetic energy
k_{factor}	Energy carry-over factor
L_{cell}	Honeycomb cell size
$\dot{m}$	Mass flow rate (leakage)
n	Number of tooth
P_n	Static pressure at outlet
P_{t0}	Total pressure at inlet
R	Ideal gas constant
Re	Reynolds number
Ri	Rotor tooth base radius
S	Source term
s	Tooth pitch
S_h	Volumetric heat generation
S_k, S_ε	User defined source terms
t	Tooth tip width
T_{t0}	Total temperature at inlet
t_w	Honeycomb wall thickness
$\vec{V}$	Velocity vector
V_r	Translational rotor speed
Y_M	Contribution of the fluctuating dilatation in compressible turbulence to the overall dissipation rate
y^+	Dimensionless wall distance

Greek letters

γ	Air specific heat ratio
ε	Turbulent dissipation
ζ	Honeycomb effect coefficient
θ	Tooth inclination angle
μ	Dynamic viscosity
μ_t	Turbulence viscosity
π	Pressure ratio
ρ	Air density
σ_k, σ_ε	Turbulent Prandtl number for k and ε